Nanoscale

Surface versus Solution Chemistry: Manipulating Nanoparticle Shape and Composition through Metal-Thiolate Interactions

Journal:	*Nanoscale*
Manuscript ID	NR-ART-09-2018-007233.R1
Article Type:	Paper
Date Submitted by the Author:	15-Nov-2018
Complete List of Authors:	Smith, Joshua; Indiana University - Bloomington, Chemistry Bunch, Connor; Indiana University - Bloomington, Chemistry Li, Yuda; Indiana University - Bloomington, Chemistry Koczkur, Kallum; Indiana University, Chemistry Skrabalak, Sara; Indiana University - Bloomington, Chemistry

Nanoscale

ARTICLE

Surface versus Solution Chemistry: Manipulating Nanoparticle Shape and Composition through Metal-Thiolate Interactions

Joshua D. Smith, Connor M. Bunch, Yuda Li, Kallum M. Koczkur, and Sara E. Skrabalak*

Received 00th January 20xx,
Accepted 00th January 20xx

DOI: 10.1039/x0xx00000x

www.rsc.org/

Nanostructures with well-defined crystallite sizes, shapes, and compositions are finding use in areas such as energy, security, and even medicine. Seeded growth is a promising strategy to achieve shape-controlled nanostructures, where specific structural features are often directed by the underlying symmetry of the seeds. Here, thiophenol derivatives capable of different metal-thiolate interactions were introduced into the synthesis of Au/Pd nanostructures by seed-mediated co-reduction. Our systematic analysis reveals that the symmetry and composition of the bimetallic nanoparticles (NPs) can be tuned as a function of additive binding strength and concentration, with symmetry reduction observed in some cases. Furthermore, additives with both thiol and amine functionalities facilitate random branching on the octahedral seed. Significantly, this synthetic versatility arises because the thiophenol derivatives modify both the surface capping of the growing nanostructures and the local ligand environment of the metal precursors, highlighting how the dual roles of synthesis components can be exploited to achieve high quality bimetallic nanostructures.

Introduction

Nanostructures with specific shapes and architectures can be accessed through seed-mediated growth processes, in which precursors are reduced in the presence of capping agents and small seeds that guide the growth process.[1–4] The variety of nanostructures that are accessible from seed-mediated growth is opening new strategies to address challenges in energy storage, security devices, chemical diagnostics, and even medical therapeutics.[5–8] The seeded synthesis of metal nanostructures often involves the reduction of metal salts in an aqueous solution containing metal seeds and hexadecyltrimethylammonium bromide (CTAB) as a capping agent.[2,9–11] Recently, organic additives that partition into the CTAB bilayer have been introduced into such syntheses to attain remarkable sample monodispersity and architectural control.[12–15] Here, various thiophenol derivatives where incorporated into the synthesis of Au/Pd nanostructures by seed-mediated co-reduction (SMCR) as a means of introducing metal-thiolate interactions that could both modulate the surface capping effect of CTAB as well as the precursor reduction process. In balancing these two types of interactions, the shape and composition of bimetallic nanostructures could be precisely controlled.

The use of organic additives in seeded syntheses are enabling some of the highest quality nanoparticle (NP) samples to be achieved. For example, Murray and co-workers demonstrated that salicylic acid derivatives could be used in the traditional synthesis of Au nanorods to improve their yield and sample monodispersity as well as to access rods with larger aspect ratios.[16] Similarly, Skrabalak and co-workers found that the same class of derivatives could be used to manipulate the tip dimensions of branched Au/Pd NPs prepared by SMCR and improve sample monodispersity for assembly.[17] Along with salicylic acid derivatives, other additives (*e.g.* amino acids, hydroquinone, sodium oleate, etc.) have been introduced to NP systems to improve both yield and morphological control.[15,18–21] Interestingly, little work has been done to investigate the role of thiol additives in seed-mediated syntheses where, in addition to modifying the capping of the growing nanostructures, these molecules are capable of binding to the metal precursors to modulate the reduction process.

Thiol derivatives are commonly used to prepare self-assembled monolayers, stabilize small metal clusters, and incorporate Raman active species.[22–25] Recent work by Nam and co-workers reported concave Au rhombic dodecahedra from the overgrowth of Au cuboctahedral seeds in the presence of 4-aminothiophenol (4-ATP).[26] These NPs displayed enhanced catalytic activity which was attributed to the considerable surface area of high-index facets stabilized by 4-ATP.[26] Furthermore, changing the strength of the Au–S interaction at the nanoparticle surface through the use of thiophenols with different substituents induced dramatic changes in morphology.[26] This study, and others, highlight how thiophenol derivatives interact with metal surfaces; however, these molecules are also capable of coordinating with metal cations to form thiophenolates, which may affect the growth process in other ways as well.[16,27–29]

Here, the effect of thiophenol derivatives on the shape and composition of Au/Pd nanostructures prepared by SMCR as a model bimetallic system was systematically studied. SMCR is a

Indiana University, Department of Chemistry, 800 E. Kirkwood Ave., Bloomington, IN 47405, USA.
Electronic Supplementary Information (ESI) available. See DOI: 10.1039/x0xx00000x

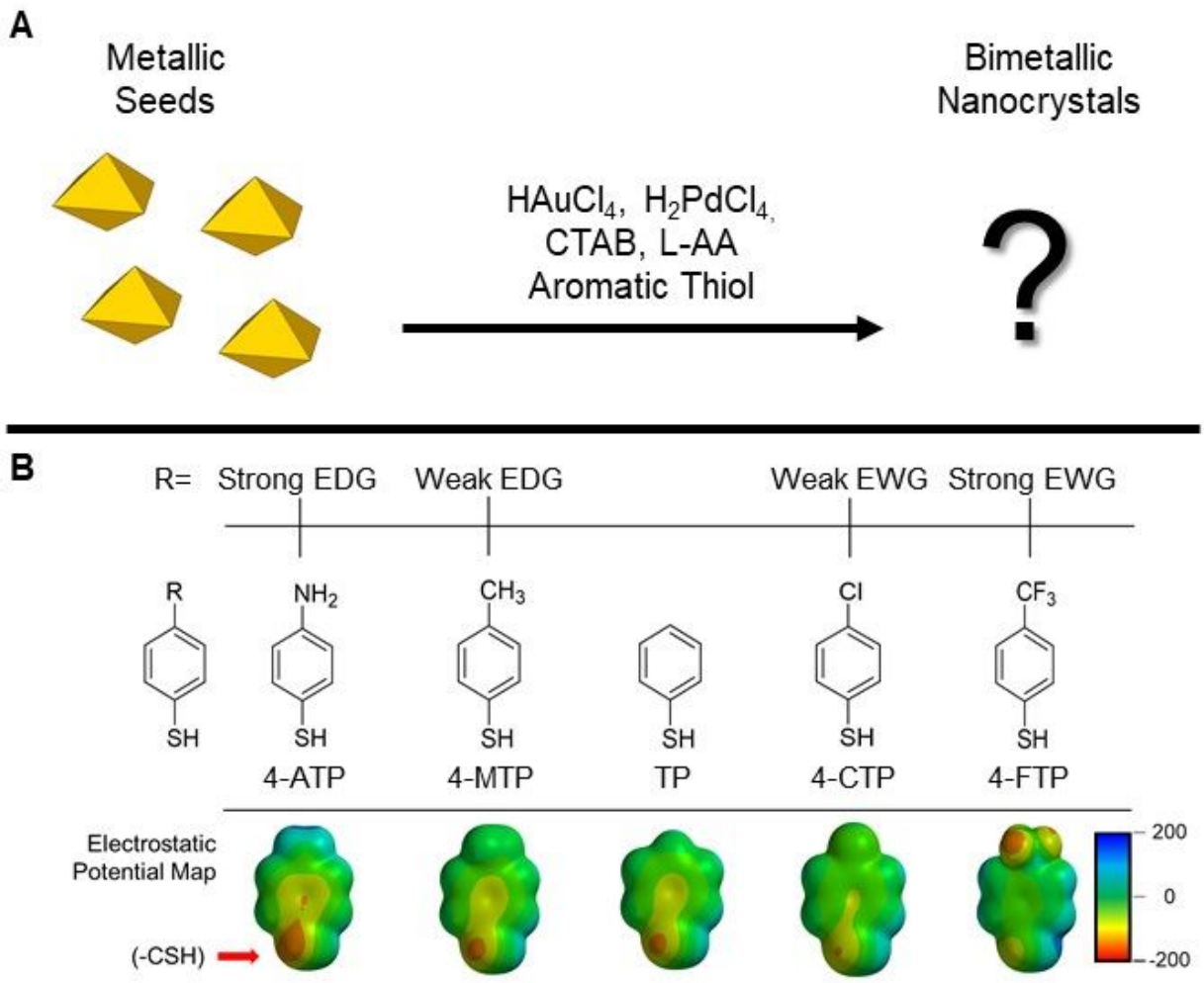

Fig. 1 (a) Schematic demonstrating the components involved in the synthesis of bimetallic nanocrystals during seed-mediated co-reduction and (b) calculated electrostatic potential maps of various thiophenol derivatives that were added. Color scale bar ranges from 200 kJmol-1 (blue) to negative 200 kJmol-1 (red).

robust method for accessing Au/Pd NPs of different morphologies, where Au and Pd precursors are co-reduced simultaneously with L-ascorbic acid in the presence of shape-controlled Au seeds and CTAB; in this case, various thiophenol derivatives were studied and the results analysed as a function of metal-thiol binding strength and additive concentration.[30–32] Our analysis reveals that the symmetry and composition of bimetallic NPs grown from Au octahedral seeds can be manipulated effectively by changing these synthetic features. Overall, these studies present new guidelines for the use of thiol-based additives in seed-mediated syntheses and demonstrate that concepts from organometallic and surface chemistry can be applied predictably to the synthesis of complex nanostructures.

Results and Discussion

Synthetic Strategy and Considerations with Thiol Additives.

4-ATP, 4-methylthiophenol (4-MTP), thiophenol (TP), 4-chlorothiophenol (4-CTP), and 4-trifluoromethylthiophenol (4-FTP) were systematically studied as additives in the synthesis of bimetallic structures from octahedral Au seeds, with the process depicted in Fig. 1a. These additives were selected because the strength of metal-thiolate interactions should depend on the electron withdrawing/donation effect from the para-substituent.[26,33] Electrostatic potential maps of each thiophenol derivative are shown in Fig. 1b, where the thiol of 4-ATP is the most electron rich and the thiol of 4-FTP is the most electron poor. These results are in agreement with Hammett substitution theory in which the electron donating/withdrawing behavior of the functional groups influence the electron density at the thiol position.[34] Given that changing the electron density of the thiol group will drastically effect the metal-thiolate binding strength as revealed by DFT calculations in Table S1, each additive was studied over a range of concentrations.[33,35] It is important to note that the pH and ionic strength changes in the growth solution are not large enough to account for the

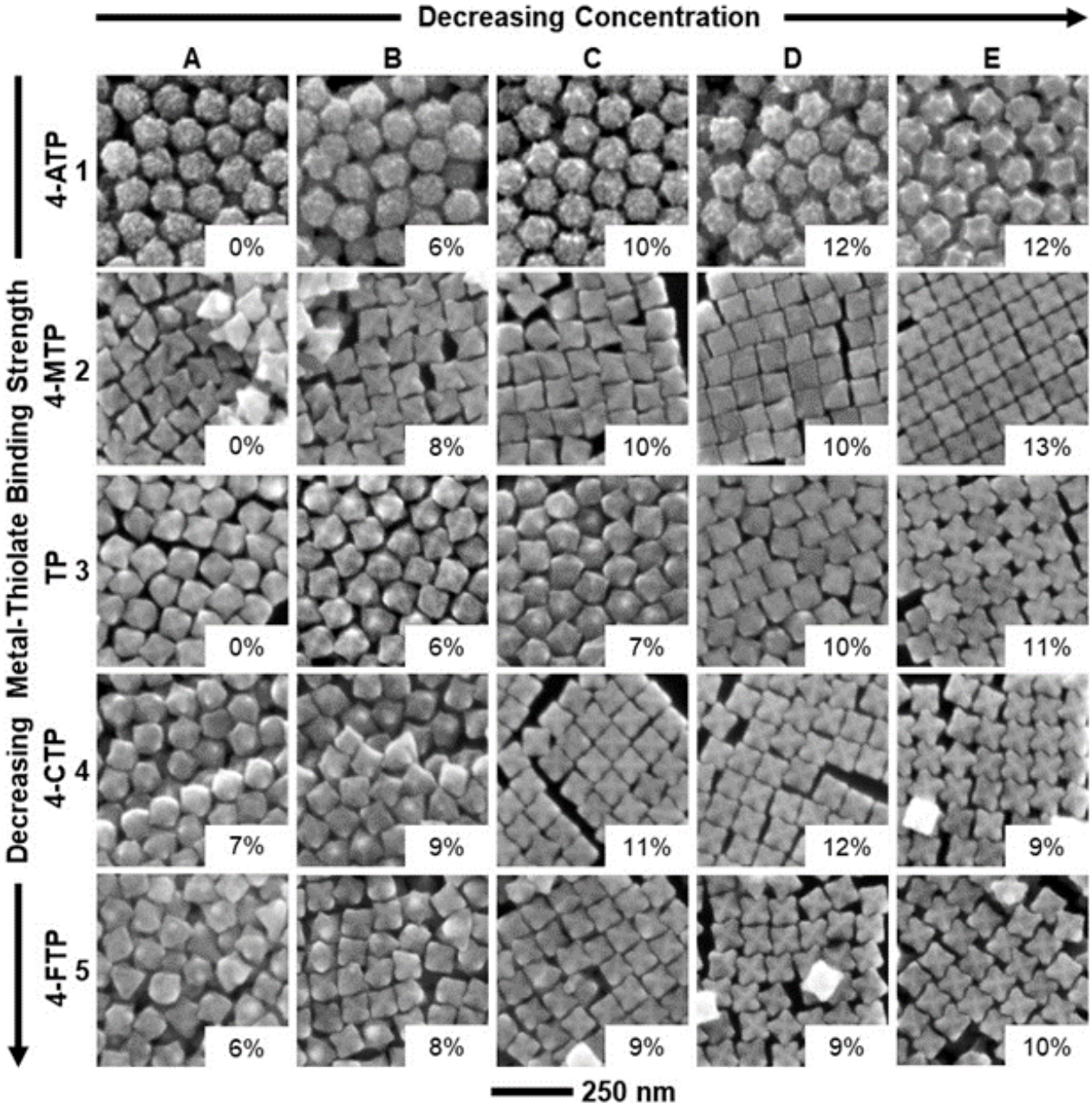

Fig. 2 SEM with inset Pd percentage from EDS of 4-aminothiophenol (row 1), 4-methylthiopehnol (row 2), thiophenol (row 3), 4-chlorothiophenol (row 4), and 4-trifluoromethylythiopenol (row 5) at 30 µM (column A), 20 µM (column B), 10 µM (column C), 5 µM (column D), and 1 µM (column E) concentrations. EDS vary by about 1%.

changes to the final shape and composition of the synthesized NPs.[30]

Influence of Thiophenol Derivatives on NP Shape.

Scanning electron microscopy (SEM) of octahedral Au seeds and the products obtained during additive-free SMCR (8-branched Au/Pd nanostructures with O_h symmetry, as previously reported)[36,37] are shown in Fig. S1 and Fig. S2, respectively. SEM images of the products prepared with different thiophenol derivatives at different concentrations are shown in Fig. 2 (lower magnification images in Fig. S3) along with the atomic Pd% in the Au/Pd NPs (determined from SEM-EDS) denoted in the lower right of each image (Table S2 for multi-sample statistical analysis). This data is supported with inductively coupled plasma mass spectrometry (ICP-MS) of samples A2-5, with trace amounts of Pd (below the detection limit of SEM-EDS) being detected for the samples prepared with TP and 4-MTP (Fig. S4). Some deviations in structure and composition compared to the additive-free results are evident, as discussed fully shortly. The columns (from left to right) correspond to

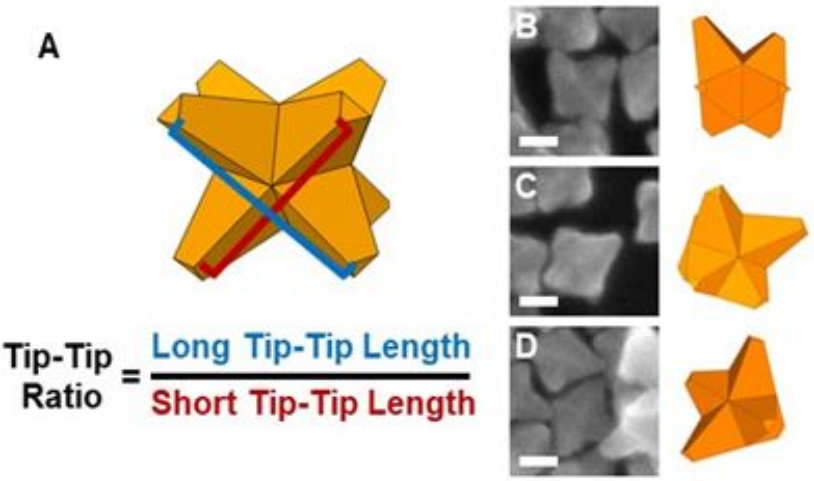

F Additive	Percent of Particles with Reduced Symmetry	Tip-Tip Ratio
Control	1.3%	1.02
4-MTP	48.9%	1.23
TP	24.6%	1.11
4-CTP	12.2%	1.06
4-FTP	5.9%	1.04

Fig. 3 Quantative analysis of the anisotorpy in select samples where (a) illustrates how the tip-tip ratio was cacluated and scanning electron micrographs with models of (b-d) illustrate branched nanoparticles with different modes of symmtery reudction A summary of tip-tip ratio and percent particles with symmetry reduction is found in (f). The percent of symmetry reduced particles was determined by the number of particles in which one diagnonal tip-tip length was at least 5 nm longer than the other. All scale bars are 50 nm.

products prepared with decreasing concentration of additive and the rows correspond to different thiophenol derivatives. Various data sets presented within this chapter will be referred to as "Fig. X CN", where X is the Fig. number and C is the column letter and N is the row number within that figure.

Additive concentrations were varied from 30 µM to 1 µM in Fig. 2, where Column A is 30 µM, Column B is 20 µM, Column C is 10 µM, Column D is 5 µM, and Column E is 1 µM. Regardless of the metal-thiolate strength, an increase in additive concentration results in a decrease in the atomic Pd% in the final nanostructure compared to when no additive is used in the synthesis. These increases in additive concentration are also coupled with changes in morphology, with less defined branching at higher concentrations of 4-MTP, 4-TP, 4-CTP, and 4-FTP and the addition of 4-ATP producing completely new structures. In the case of 4-ATP, which corresponds to the strongest metal-thiolate interactions, rhombic dodecahedra are largely produced at low concentrations and nanostructures with many randomly positioned branches are produced at higher concentrations. Interestingly, those additives capable of stronger metal-thiolate interactions produce more dramatic changes in morphology at lower concentrations. For example, Au-Pd octopods are achieved at the high concentrations of 4-FTP studied (Fig. 2 B5), but octopods are not observed at the lowest concentrations of 4-ATP studied (Fig. 2 E1). The sensitivity of the system to strongly binding additives is especially evident for 4-ATP in which octopodal structures were not produced until its concentration was decreased to 80 nM (Fig. S5). In general, stronger metal-thiolate interactions drive more drastic changes in both the architecture and composition of the final NPs. We note that ICP-MS results for samples A2-A5 show an increase in the % sulfur with increasing additive binding strength, indicative of more bound thiol (Fig. S4).

Examining the results in Fig. 2 more closely, symmetry reduction is evident through the use of additives. A hallmark feature of seeded syntheses is that the symmetry of the seeds is often transferred to the final product.[1,2,9] In the case of 4-ATP, random branching is obvious. However, from Fig. 2 B2-5, 8-branched octopodal structures are apparent but varying reductions in symmetry (*i.e.,* notable deviation from O_h

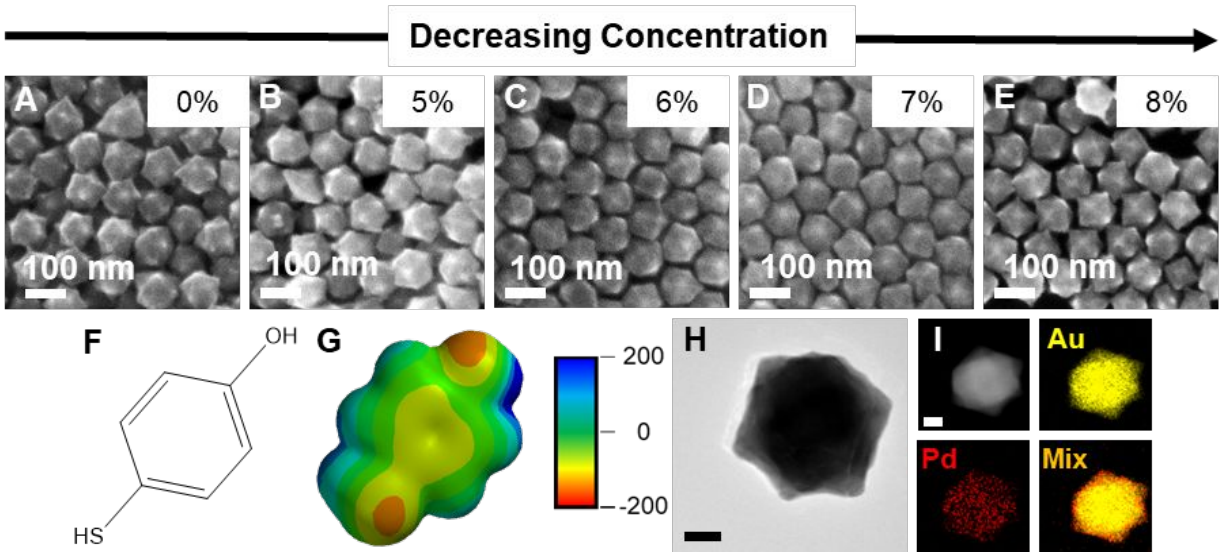

Fig. 4 SEM and EDS insets (Pd% with an average deviation of 1%) of products obtained at (a) 30 μM, (b) 20 μM, (c) 10 μM, (d) 5 μM , (e) and 1 μM concentrations of 4-hydroxythiophneol along with (f) skeletal structure and g) electrostatic potential maps in terms of $kJmol^{-1}$. TEM and STEM-EDS of a single particle can be seen in (h) and (i) respectively. Unless noted, all scale bars are 25 nm.

symmetry) are also evident depending on the additive. NP symmetry reduction was quantified by comparing the tip-tip distance between branches at opposite corners (*i.e.*, diagonal tip-tip length). The degree of symmetry reduction was obtained by taking the ratio of the long tip-tip length to the short tip-tip length as defined by Fig. 3a. If the NP has a tip-tip ratio of at least 1.05, then the NP was considered symmetrically reduced (*i.e.,* no longer O_h). This analysis revealed that 4-MTP produced the most particles with reduced symmetry and the greatest degree of symmetry reduction (48.9% of particles at a ratio of 1.23 compared to 1.3% at 1.02 for the control/additive-free results). In fact, the number of symmetry reduced particles and the magnitude of symmetry reduction correlates with the anticipated strength (Table S1) of metal-thiolate interactions, with 4-FTP causing the least amount of change (Fig. 3f).

Methods that enable controlled symmetry reduction in nanosyntheses are highly sought after as they offer new ways to manipulate the physicochemical properties of NPs for catalysis, sensing, and optic devices.[38–40] Here, we propose clusters of aromatic thiols unequally passivate crystallographically identical nucleation sites, thus promoting site-dependent growth kinetics that results in symmetry reduction of the final NP. This hypothesis is reasonable given that i) islands of aromatic thiols form readily at high energy sites (where vertices can have atomically different defect populations while still being crystallographically equivalent), ii) the kinetics of heterogenous nucleation are dependent on the displacement of bound capping agents, and iii) the concentration of thiophenol derivatives is low.[22,41,42] Furthermore, the rate of heterogenous nucleation is inversely proportional to the bond strength of the capping agent in which the displacement of weakly coordinating thiophenol derivatives desorb faster than more strongly bound derivatives.[42,43] This hypothesis is supported (Fig. 3) in which the thiophenol derivative with strongest metal-thiolate interactions (Table S1) promote the largest reduction in branch symmetry.

Of the aromatic thiols used as additives, 4-ATP induced the most drastic changes in the final NP morphology, which is attributed to the strong metal-thiolate interaction. To investigate this further, 4-hydroxythiophenol (4-HTP) was used due to the strong electron donating character of the hydroxyl functional group at the para position. SEM, TEM, and STEM-EDS of the prepared structures can be seen in Fig. 4. Symmetrically branched octopodal structures were produced but the branches were shorter than those from the control (additive-free) experiment (a tip-tip length of 94±9 nm and an aspect ratio of 1.05 versus tip-tip length of 112±5 nm and an aspect ratio of 1.02). Like the other derivatives, as the concentration of the thiol increases in the synthesis, the concentration of Pd in the NPs decreases and is distributed similarly as revealed by STEM-EDS (Fig. 4h,i). The Hartree-Fock approximation of 4-MTP shows high electron density at the thiol position, similar to what was observed for 4-ATP (Fig. 4g). While the metal-thiolate interaction strength may be like others in this study, 4-HTP is the only aromatic thiol studied that is miscible in water alone. This difference allows for faster desorption and improved solution mobility of 4-HTP compared to other aromatic thiol additives.[43] The increased solution mobility and faster desorption kinetics may account for the retention of NP symmetry. As the degree of branch length can vary so dramatically with the nature of the para-substituent, final branched NPs obtained from 4-HTP and 4-ATP were vastly different. Further investigation was done to understand the influence of the functional group at the para position.

The role of the amine was investigated by using 2-aminothiophenol (2-ATP) and aniline. Skeletal structures of

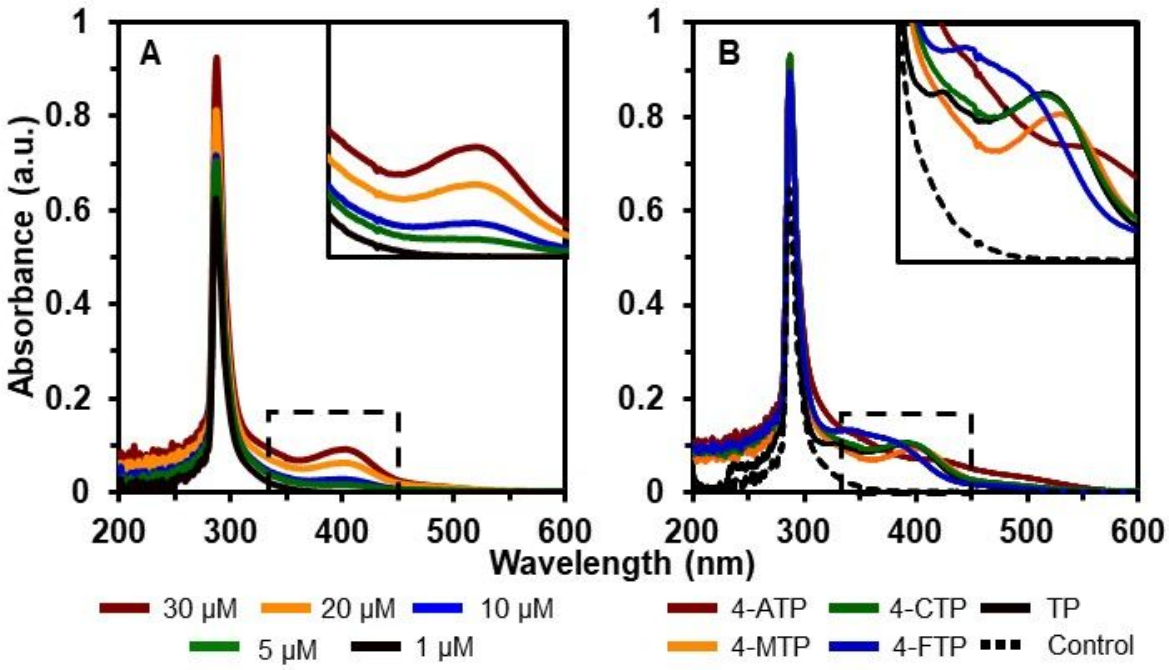

Fig. 5 UV-visible spectra (water) of supernatants with (a) different concentrations of 4-methylthiophenol (4-MTP) and (b) different thiophenol derivatives at 30 μM. Inset of the spectra from 325-450 nm.

each additive are presented in Fig. S6. SEM micrographs presented in Fig. S6 corresponds to results obtained where row 1 corresponds to 2-ATP and row 2 to aniline. The columns present in Fig. S6 correspond to the same concentrations for the columns in Fig. 2. Micrographs of NPs obtained using 2-ATP are similar to what was observed when 4-ATP was used, but the final structures appeared less sensitive to higher concentrations of 2-ATP given that Fig. S6 E1 yields octopodal structures. The decrease in sensitivity may arise from steric hindrance of the amine group at the ortho position or synergistic surface capping.[44]

When aniline was introduced as an aromatic additive, no major structural changes were observed. The lack of structural change is indicative of the aromatic amine is not the major contribution to the final NPs structure. This finding was further supported by comparing the morphology of NPs prepared with 1-dodecanethiol and 1-dodeclyamine additives (Fig. S7). The introduction of dodecanethiol produced well defined cubes where dodecylamine facilitated no structural changes in the NPs compared to the control results which produced octopods. In general, one must consider the strength of metal-thiolate interaction and the possible secondary interactions from other functional groups present in the organic additive.

Influence of Thiophenol Derivatives on NP Composition.

Beyond modifying NP shape, the addition of thiophenol derivatives to the synthesis of Au/Pd NPs by SMCR can modify the atomic %Pd incorporated into the NPs as summarized in Fig. 2 and Table S1. In general, the greater the concentration of derivatives in a synthesis, the lower the Pd content in the final structure. This decrease in Pd incorporation arises from coordination of the thiophenol derivatives preferentially with the Pd salt. This claim is supported by analysis of the reaction supernatants, which have a yellow color (Fig. S8). UV-visible spectroscopy was used to analyze the supernatants, with spectra displaying two major peaks (Fig. 5); one centered at 287 nm and a second centered between 325 nm and 450 nm depending on the additive used (inset of Fig. 6b). The first corresponds to the Pd and Au precursors.[30] The second peak corresponds to Pd-thiophenol complexes.[45] This peak assignment is reasonable given synthesis of branched NPs in the absence of Pd have colorless supernatants (Fig. S9) and show no absorbance between 325 nm and 450 nm (Fig. S10) The loss of Pd is accounted for in Fig. 6a in which decreasing the concentration of 4-MTP results in a decrease in absorbance intensity at 407 nm. This decrease in absorbance indicates a loss in Pd-thiolate complexes; thus more Pd precursor is available for heterogenous nucleation. Spectra in Fig. 6b corresponds to Pd-thiophenol complexes with 4-ATP having a peak absorbance at 420 nm, 4-MTP at 407 nm, TP at 393 nm, 4-CTP at 388 nm, and 4-FTP at 343 nm. In the absence of a thiophenol derivative, only the feature at 287 nm is observed. Similar to 4-MTP, decreasing the concentration of each additive corresponds to a decrease in peak absorbance intensity (Fig. S11).

TEM and STEM-EDS for the products in Fig. 2 Column B are in Fig. 6. Pd deposition is similar to what has been previously observed for SMCR, with Pd enriched at the surfaces of the NPs.[1] The incorporation of Pd into Au structures provides high refractive index sensitivity, the possibility for plasmon-enhanced catalysis, surface enhanced Raman spectroscopy of Pd-catalyzed processes, and more.[46–48] More importantly for

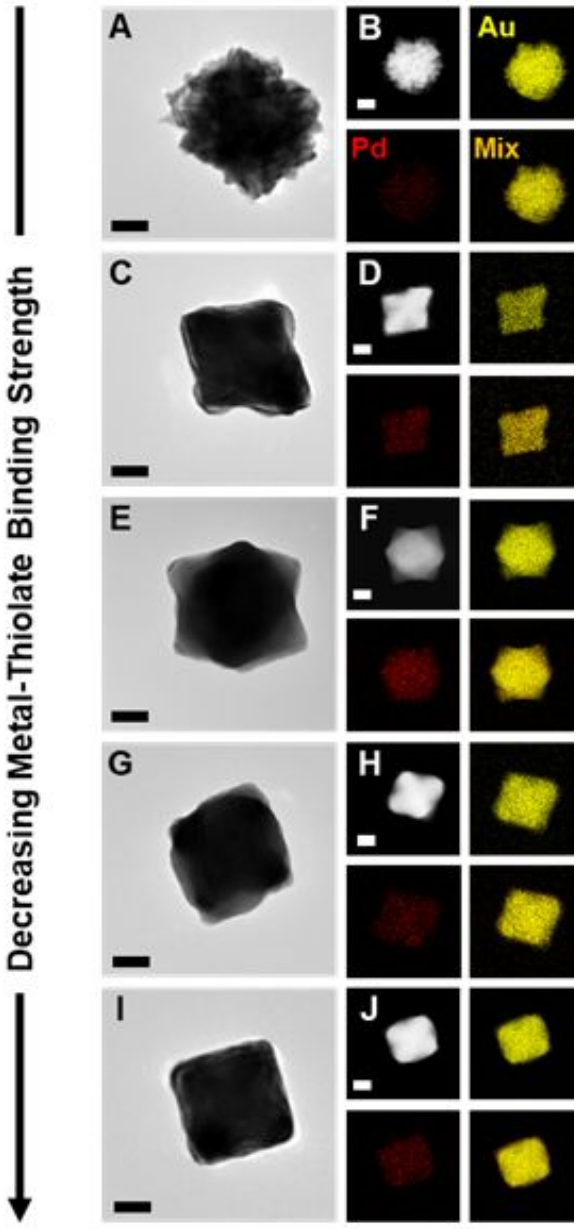

Fig. 6 TEM and STEM-EDS of (a,b) 4-aminothiophenol, c,d) 4-methylthiophenol, (e,f) thiophenol, (g,h) 4-chlorothiophenol, and (i,j) 4-trifluoromethylthiophenol. All scale bars are 25 nm. Pd and Au are represented by red and yellow in elemental

this study, the incorporation of Pd into branches stabilizes the branched structure by retarding surface diffusion.[1] This role of Pd is supported by a study in which the amount of Pd precursor in the synthesis was decreased, and ultimately completely omitted. In all cases, nanocrystals with O_h symmetry were obtained; however, eight-branched structures gradually transition to cubes (Fig. S12). In contrast, SEM micrographs in Fig. S13 show that branched NPs are obtained when 4-ATP and TP are introduced at different concentrations in the absence of Pd precursor. This finding suggests that the strong Au-thiol interaction inhibits surface diffusion of Au adatoms and stabilizes the structures.

Conclusions

Here, thiophenol-based additives, that form metal-thiolate interactions on the seed surface and with the metal precursor in solution, were introduced into a model SMCR system to manipulate the shape and composition of branched Au/Pd NPs. Systematic changes in the thiophenol structure and concentration provided synthetic handles for simultaneously controlling the symmetry and composition of the final NP. Interestingly, strongly bound aromatic thiols result in the largest symmetry reduction. Symmetry reduction was evident in which strongly bound 4-ATP produced asymmetric NPs with randomly dispersed branching and 4-FTP (weaker metal-thiolate interactions) yielded symmetrically branched octopodal structures. Along with the desorption kinetics of the thiol from the surface, the strength of the metal-thiophenolate interaction in solution is important to consider as a versatile handle to manipulating the final composition of the NP.

Overall, this work displays the importance of considering the multiple roles additives can have on nanosyntheses, including the strength of surface interaction, degree of surface capping, and the possibility of solution chemistry. Although this list is not exhaustive, researchers should also consider the influence of additives on the packing of capping agents, self-assembly of monolayers, and the reducing capabilities.[12,13,16] The results presented here are expected to provide new guidelines for the manipulation of synthetic conditions to prepare complex nanostructures with tunable symmetries and composition..

Conflicts of interest

There are no conflicts to declare.

Acknowledgements

The authors would like to thank Nicholas Daanen and Matthew Gordon for their assistance in interpreting the spectroscopic shifts and Joseph Burkhart with the preparation of models. In addition, the authors would like to thank the staff of the Nanoscale Characterization Facility (Dr. Yi Yi) and Electron Microscopy Center (Dr. David Morgan and Dr. Barry Stein) at Indiana University for their continued support. This work was funded by the National Science Foundation (award number: CHE-1602476).

Notes and References

‡ Chemicals, characterization techniques, experimental procedures, and supplemental figures can be found in the supplemental information.

1 R. G. Weiner, M. R. Kunz and S. E. Skrabalak, *Acc. Chem. Res.*, 2015, **48**, 2688–2695.

2 Y. Xia, K. D. Gilroy, H. C. Peng and X. Xia, *Angew. Chem. Int. Ed.*, 2017, **56**, 60–95.
3 M. Grzelczak, J. Pérez-Juste, P. Mulvaney and L. M. Liz-Marzán, *Chem. Soc. Rev.*, 2008, **37**, 1783–1791.
4 Y. Xia, Y. Xiong, B. Lim and S. E. Skrabalak, *Angew. Chem. Int. Ed.*, 2009, **48**, 60–103.
5 S. E. Lohse and C. J. Murphy, *J. Am. Chem. Soc.*, 2012, **134**, 15607–15620.
6 X. Huang, P. K. Jain, I. H. El-Sayed and M. A. El-Sayed, *Lasers Med Sci*, 2008, **23**, 217.
7 K. A. Willets and R. P. V. Duyne, *Annu. Rev. Phys. Chem.*, 2007, **58**, 267–297.
8 A. F. Smith and S. E. Skrabalak, *J. Mater. Chem. C*, 2017, **5**, 3207–3215.
9 E. Ye, M. D. Regulacio, S.Y. Zhang, X. Jun Loh and M.Y. Han, *Chem. Soc. Rev.*, 2015, **44**, 6001–6017.
10 B. Lim and Y. Xia, *Angew. Chem. Int. Ed.*, 2011, **50**, 76–85.
11 M. L. Personick and C. A. Mirkin, *J. Am. Chem. Soc.*, 2013, **135**, 18238–18247.
12 Y. Xu, X. Wang, L. Chen, Y. Zhao, L. He, P. Yang, H. Wu, F. Bao and Q. Zhang, *J. Mater. Chem. C*, 2015, **3**, 1447–1451.
13 N. Ortiz, S. J. Hong, F. Fonseca, Y. Liu and G. Wang, *J. Phys. Chem. C*, 2017, **121**, 1876–1883.
14 P. J. Straney, N. A. Diemler, A. M. Smith, Z. E. Eddinger, M. S. Gilliam and J. E. Millstone, *Langmuir*, 2018, **34**, 1084–1091
15 H. E. Lee, H. Y. Ahn, J. Mun, Y. Y. Lee, M. Kim, N. H. Cho, K. Chang, W. S. Kim, J. Rho and K. T. Nam, *Nature*, 2018, **556**, 360–365.
16 X. Ye, L. Jin, H. Caglayan, J. Chen, G. Xing, C. Zheng, V. Doan-Nguyen, Y. Kang, N. Engheta, C. R. Kagan and C. B. Murray, *ACS Nano*, 2012, **6**, 2804–2817.
17 C. J. DeSantis, A. C. Sue, A. Radmilovic, H. Liu, Y. B. Losovyj and S. E. Skrabalak, *Nano Lett.*, 2014, **14**, 4145–4150.
18 X. Ye, C. Zheng, J. Chen, Y. Gao and C. B. Murray, *Nano Lett.*, 2013, **13**, 765–771.
19 K. I. Requejo, A. V. Liopo, P. J. Derry and E. R. Zubarev, *Langmuir*, 2017, **33**, 12681–12688.
20 J. E. Millstone, W. Wei, M. R. Jones, H. Yoo and C. A. Mirkin, *Nano Lett.*, 2008, **8**, 2526–2529.
21 J. Li, W. Wang, X. Zhang, H. Yao, Z. Wei, X. Li, X. Mu, J. Jiang and H. Zhang, *RSC Adv.*, 2018, **8**, 21316–21325.
22 Q. Jin, J. A. Rodriguez, C. Z. Li, Y. Darici and N. J. Tao, *Sur. Sci.*, 1999, **425**, 101–111.
23 M. Zhu, C. M. Aikens, F. J. Hollander, G. C. Schatz and R. Jin, *J. Am. Chem. Soc.*, 2008, **130**, 5883–5885.
24 P. D. Jadzinsky, G. Calero, C. J. Ackerson, D. A. Bushnell and R. D. Kornberg, *Science*, 2007, **318**, 430–433.
25 M. A. Bryant, S. L. Joa and J. E. Pemberton, *Langmuir*, 1992, **8**, 753–756.
26 H.-E. Lee, K. D. Yang, S. M. Yoon, H.-Y. Ahn, Y. Y. Lee, H. Chang, D. H. Jeong, Y.-S. Lee, M. Y. Kim and K. T. Nam, *ACS Nano*, 2015, **9**, 8384–8393.
27 L. D. Marks and L. Peng, *J. Phys.: Condens. Matter*, 2016, **28**, 053001.
28 Y. Xia, X. Xia and H.-C. Peng, *J. Am. Chem. Soc.*, 2015, **137**, 7947–7966.
29 Y. Wang, H.-C. Peng, J. Liu, C. Z. Huang and Y. Xia, *Nano Lett.*, 2015, **15**, 1445–1450.
30 C. J. DeSantis, A. C. Sue, M. M. Bower and S. E. Skrabalak, *ACS Nano*, 2012, **6**, 2617–2628.
31 M. R. Langille, J. Zhang, M. L. Personick, S. Li and C. A. Mirkin, *Science*, 2012, **337**, 954–957.
32 Sanedrin R. G., Georganopoulou D. G., Park S. and Mirkin C. A., *Adv. Mater.*, 2005, **17**, 1027–1031.
33 S. Miranda-Rojas, A. Muñoz-Castro, R. Arratia-Pérez and F. Mendizábal, *Phys. Chem. Chem. Phys.*, 2013, **15**, 20363–20370.
34 Louis P. Hammett, *J. Am. Chem. Soc.*, 1937, **59**, 93–103.
35 P. Carro, G. Corthey, A. A. Rubert, G. A. Benitez, M. H. Fonticelli and R. C. Salvarezza, *Langmuir*, 2010, **26**, 14655–14662.
36 C. J. DeSantis, A. A. Peverly, D. G. Peters and S. E. Skrabalak, *Nano Lett.*, 2011, **11**, 2164–2168.
37 C.-C. Chang, H.-L. Wu, C.-H. Kuo and M. H. Huang, *Chem. Mater.*, 2008, **20**, 7570–7574.
38 S. Chen, S. V. Jenkins, J. Tao, Y. Zhu and J. Chen, *J. Phys. Chem. C*, 2013, **117**, 8924–8932.
39 H. Yu, Y. Jiao, N. Li, J. Pang, W. Li, X. Zhang, X. Li and C. Li, *Appl. Surf. Sci.*, 2018, **427**, 771–778.
40 W. Zhang, J. Liu, W. Niu, H. Yan, X. Lu and B. Liu, *ACS Appl. Mater. Interfaces*, 2018, **10**, 14850–14856.
41 C. Vericat, M. E. Vela, G. Benitez, P. Carro and R. C. Salvarezza, *Chem. Soc. Rev.*, 2010, **39**, 1805–1834.
42 A. N. Chen, M. M. Scanlan and S. E. Skrabalak, *ACS Nano*, 2017, **11**, 12624–12631.
43 Gabor A. Somorjai and Yimin Li, *Introduction to Surface Chemistry and Catalysis*, Wiley, 2nd edn., 2010.
44 W. Niu, Y. A. A. Chua, W. Zhang, H. Huang and X. Lu, *J. Am. Chem. Soc.*, 2015, **137**, 10460–10463.
45 Z. Yang, A. B. Smetana, C. M. Sorensen and K. J. Klabunde, *Inorg. Chem.*, 2007, **46**, 2427–2431.
46 A. F. Smith, S. M. Harvey, S. E. Skrabalak and R. G. Weiner, *Nanoscale*, 2016, **8**, 16841–16845.
47 Zhang Lin-Fei, Zhong Sheng-Liang and Xu An-Wu, *Angew. Chem. Int. Ed.*, 2012, **52**, 645–649.
48 F. Wang, C. Li, H. Chen, R. Jiang, L.D. Sun, Q. Li, J. Wang, J. C. Yu and C.H. Yan, *J. Am. Chem. Soc.*, 2013, **135**, 5588–5601.

